RARE METALS

ORIGINAL ARTICLE

Room-temperature ionic conductivity of Ba, Y, Al co-doped $Li_7La_3Zr_2O_{12}$ solid electrolyte after sintering

Xiao-Zhen Liu*, Lei Ding, Yu-Ze Liu, Li-Ping Xiong, Jie Chen, Xiao-Long Luo

Abstract The Ba, Y and Al co-doped $Li_7La_3Zr_2O_{12}$ (LLZO) was prepared by the solid-state reaction method. Effect of sintering on the crystallographic structure, morphology, total conductivity, relative density and contractibility rate of the prepared solid electrolyte was studied, respectively. The sintered samples were characterized by X-ray diffractometer (XRD), scanning electron microscopy (SEM), electrochemical impedance spectra (EIS) and inductively coupled plasma atomic emission spectrometry (ICP-AES) techniques, respectively. The cubic garnet phase Ba, Y and Al co-doped LLZO is obtained, and the room-temperature total conductivity of the Ba, Y and Al co-doped LLZO solid electrolyte is improved significantly by eliminating the grain boundary resistances and improving the densifications with controlling sintering temperature (T) and time (t), respectively. Sintering at 1160–1190 °C for 12 h and at 1190 °C for 6–15 h, respectively, the Ba, Y and Al co-doped LLZO solid electrolytes are cubic garnet phase. Sintering at 1180–1190 °C for 12 h and at 1190 °C for 12–18 h, respectively, SEM images of the cross section of the Ba, Y and Al co-doped LLZO solid electrolytes exhibit the distinctively flattened morphology without any noticeable grain boundaries. The total conductivity, relative density and contractibility rate of $Li_{6.52}La_{2.98}Ba_{0.02}Zr_{1.9}Y_{0.1}Al_{0.2}O_{12}$ solid electrolyte are 2.96×10^{-4} S·cm^{-1}, 94.19% and 18.61%, respectively.

Keywords Solid electrolyte; Ionic conductivity; Sintering; $Li_7La_3Zr_2O_{12}$; Garnet

1 Introduction

The organic Li-ion salt electrolytes are widely used in lithium-ion batteries at present, but their flammability may cause serious safety issues [1–7], and the stability problem of the aqueous electrolytes with lithium metal has seriously limited the voltage range [2]. Therefore, inorganic solid-state electrolytes are now attracting much attention. Garnet-type $Li_7La_3Zr_2O_{12}$ (LLZO) as the inorganic solid electrolyte has excellent thermal performance, high chemical compatibility against molten lithium, high conductivity, wide electrochemical window and has been given much attention [8–15]. LLZO has cubic and tetragonal crystalline phases. The lithium-ion conductivity of cubic phase LLZO is about 2 or 3 orders of magnitude higher than that of tetragonal phase LLZO [16]. Hence, formation and stabilization of cubic phase is an effective approach for increasing the total conductivity of LLZO. Ga [17], Al [18–20], W [21], Ta [1, 3, 22], Nb [23], Sc [24], Hf [24, 25], Ti [26], Te [27], etc., were doped in LLZO, respectively, to stabilize the cubic structure of LLZO by previous researchers. Our research found that the room-temperature ionic conductivities of LLZO could be improved significantly by the co-doping of Ba, Y and Al in LLZO [28]. In addition, minimizing the grain boundary resistance is also an effective approach for enhancing the total conductivity in this solid electrolyte [24].

X.-Z. Liu*, L. Ding, L.-P. Xiong, X.-L. Luo
School of Chemical and Environmental Engineering, Shanghai Institute of Technology, Shanghai 201418, China
e-mail: liuxiaozhen5291@163.com

Y.-Z. Liu
College of Economic and Management, Beijing Forestry University, Beijing 100083, China

J. Chen
Regenia AB, Stockholm 10691, Sweden

In this paper, the Ba, Y and Al co-doped LLZO was prepared by the solid-state reaction method. Effect of sintering on the crystallographic structure, morphology, total conductivity, relative density and contractibility rate of the prepared solid electrolyte was studied, respectively. The sintered samples were characterized by X-ray diffraction (XRD), scanning electron microscopy (SEM), electrochemical impedance spectroscopy (EIS) and inductively coupled plasma atomic emission spectrometry (ICP-AES) techniques, respectively.

2 Experimental

2.1 Preparation of solid electrolyte sample

Samples of Ba, Y and Al co-doped LLZO (composition: $Li_{6.52}La_{2.98}Ba_{0.02}Zr_{1.9}Y_{0.1}Al_{0.2}O_{12}$) were prepared by solid-state reaction method in the literature [28]. Stoichiometric amounts of Li_2CO_3 (analytical reagent (AR) grade), La_2O_3 (99.999%), $BaCO_3$ (AR), ZrO_2 (AR), Y_2O_3 (99.999%) and Al_2O_3 (99.999%) were selected as original materials. The starting materials were mixed and ball-milled for 12 h with isopropyl alcohol as the dispersing reagent and then heat-treated at 900 °C for 6 h and then ball-milled again for 12 h. Then, the obtained powder was putted into $\phi = 13$ mm model of stainless steel and pressed into pellets with 20 MPa pressure. The pellets were covered with mother powder and sintered at 1160–1200 °C for 12 h and at 1190 °C for 3–18 h, respectively, and the solid electrolyte samples were obtained.

2.2 Characterization techniques

An X-ray diffractometer (XRD, Bruker AXS D8 Advance) with Cu Kα radiation at 40 kV and 30 mA in the 2θ ranges from 10° to 60° at scanning rate of 2 (°)·min^{-1} was used to identify the phase composition of the sintered samples. The cross-sectional morphologies of the sintered samples were measured using a scanning electron microscope (SEM, HITACHI S3400N). A solartron impedance analyzer (Solartron 1260 &1287) with 100 Hz–10 MHz and 10 mV was used to identify EIS measurements of the sintered samples to measure the ionic conductivity. The relative densities of the sintered samples were measured by the Archimedes' method. The contractibility rates were measured by micrometer. The contractibility rate of the sintered sample was the ratio between contractibility value of the diameter of the sample after sintering and the diameter before sintering. Elemental analysis of sintered sample (sintering at 1190 °C for 12 h) was conducted with ICP-AES (VISTA-MPX ICP-OES) with ICP as light source.

3 Results and discussion

3.1 XRD studies

XRD patterns of Ba, Y and Al co-doped LLZO samples at different sintering temperatures are shown in Fig. 1a. The peaks are labeled with the standard pattern known as cubic garnet phase $Li_5La_3Nb_2O_{12}$ (PDF No.45–0109, the vertical lines in the bottom). From Fig. 1a, it can be seen that with temperature at 1160–1190 °C, the diffraction peaks are well matched with the standard peaks of the cubic garnet phase $Li_5La_3Nb_2O_{12}$, indicating that the solid electrolytes samples are cubic garnet phase. At 1200 °C, the sample is primarily a cubic garnet phases with small amounts of impurities such as $La_2Zr_2O_7$.

XRD patterns of Ba, Y and Al co-doped LLZO samples at different sintering times are shown in Fig. 1b. From Fig. 1b, it can be seen that as time for 3 h, along with the peaks of the cubic garnet phase sample, diffraction peak at $2\theta = 30.5°$ splits into two peaks, and there are four diffraction peaks in $50° \leq 2\theta 55°$, indicating the existence of the tetragonal garnet phase in the sample [29, 30]. And the sample is a mixture of tetragonal garnet phase and cubic garnet phases. With time for 6–15 h, the samples are cubic garnet phase. With $t = 18$ h, the sample is primarily a cubic garnet phases with small amounts of impurities such as $La_2Zr_2O_7$.
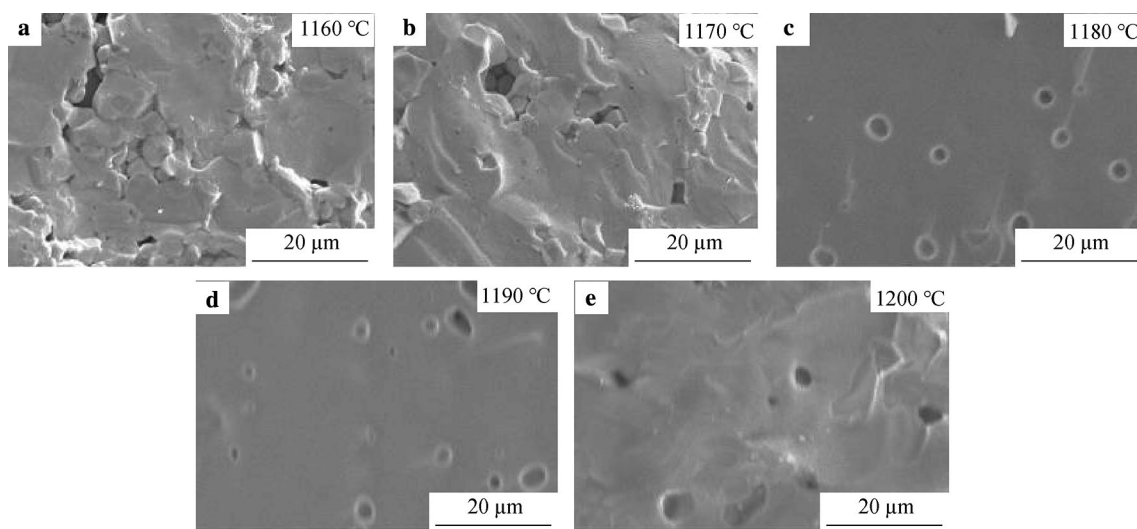
3.2 SEM image

SEM surface morphologies of the cross section of Ba, Y and Al co-doped LLZO samples at different temperatures are shown in Fig. 2. From Fig. 2, at 1160–1170 °C, the grain sizes in the samples become bigger with temperature increasing, and the grains are not in good contact with each other, implying a low density. With temperature at 1180–1190 °C, those images of the samples exhibit the distinctively flattened morphology without any noticeable grain boundaries, and the pores are observed, indicating that controlling temperature helps to eliminate the samples' grain boundary resistances and improve the densifications. Therefore, the higher densities and conductivities in the samples could be obtained by controlling temperature. The appearance of the pores could be due to the evaporation of lithium compounds. The evaporation of lithium compounds can be compensated with mother powder covering the surface during the sintering process, but the inner part cannot get completely compensation. With temperature at 1190–1200 °C, the grain sizes of the sample become smaller with temperature increasing.

SEM surface morphologies of the cross section of the Ba, Y and Al co-doped LLZO samples for different time are shown in Fig. 3. From Fig. 3, it can be seen that with
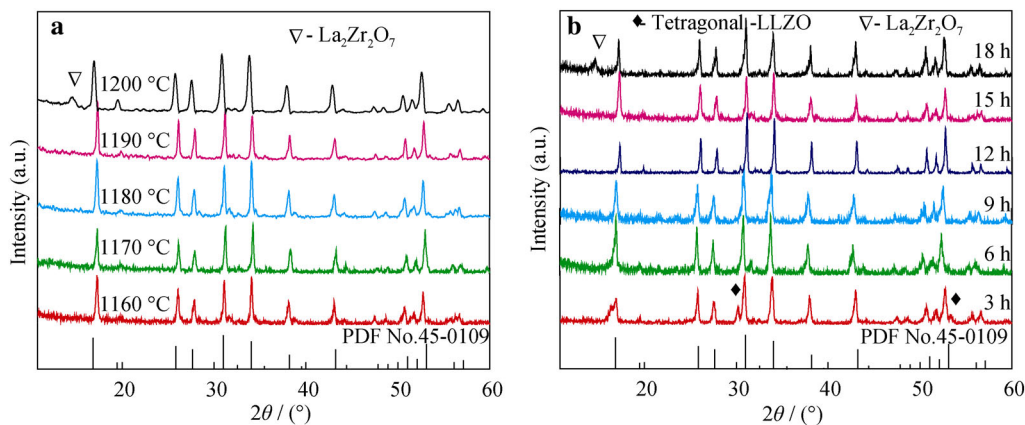
Fig. 1 XRD patterns of Ba, Y and Al co-doped LLZO samples at **a** different temperatures and **b** different times

Fig. 2 SEM images of Ba, Y and Al co-doped LLZO samples at different temperatures: **a** 1160 °C, **b** 1170 °C, **c** 1180 °C, **d** 1190 °C, and **e** 1200 °C

time for 3–9 h, the grain sizes in the samples become bigger with time increasing. With time for 12–18 h, those images of the samples exhibit the distinctively flattened morphology without any noticeable grain boundaries, and the pores become more and bigger with time increasing. Thus, the higher densities and conductivities in the samples could be obtained by controlling time.

3.3 Ionic conductivity

The impedance spectra of Ba, Y and Al co-doped LLZO samples at different temperatures measured at 25 °C in air are shown in Fig. 4a. From Fig. 4a, all the plots of the samples show only a single semicircle at high-frequency region and a remarkable diffusion tail at the low-frequency region. The semicircle represents the grain boundary impedance. The straight line corresponds to Warburg-type impedance. The bulk resistance, usually appearing at high

frequency, cannot be detected because it is out of the frequency range of the analyzer [25]. The impedance spectra were fitted with an equivalent circuit model ( ), where R and CPE1 represent the resistance and the capacitance associated with the sintered sample, respectively. CPE2 reflects the capacitance from the Ag paint current collector. The ionic conductivity (σ) was calculated using the formula: $\sigma = (1/R)\cdot(L/S)$, where σ, R, L and S represent the total ionic conductivity, total resistance obtained in EIS measurement, thickness and the effective area of the pellet, respectively. The total ionic conductivities were obtained by analyzing the impedance data with ZsimpWin software for simulation, and the values are shown in Table 1. From Table 1, σ increases significantly from 1.23×10^{-5} to 2.96×10^{-4} S·cm^{-1} with T from 1160 to 1190 °C, and due to that with temperature increasing, the grains contact better with each other. The result is supported by SEM analysis result in
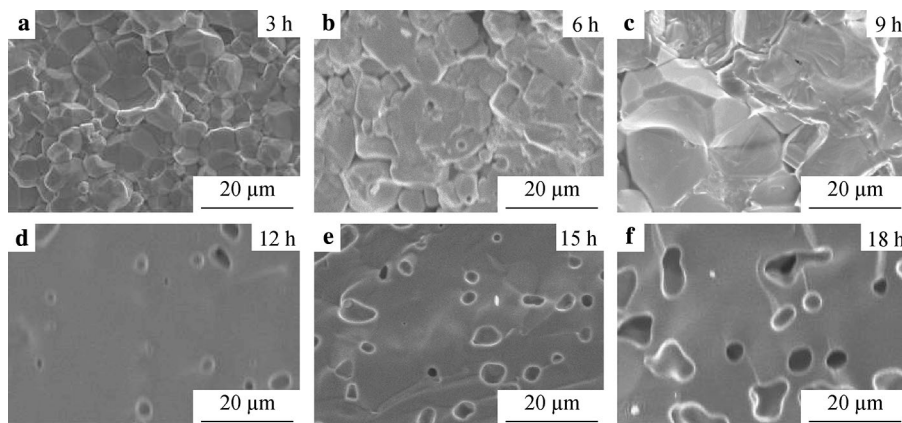
Fig. 3 SEM images of Ba, Y and Al co-doped LLZO samples at different times: **a** 3 h, **b** 6 h, **c** 9 h, **d** 12 h, **e** 15 h, and **f** 18 h
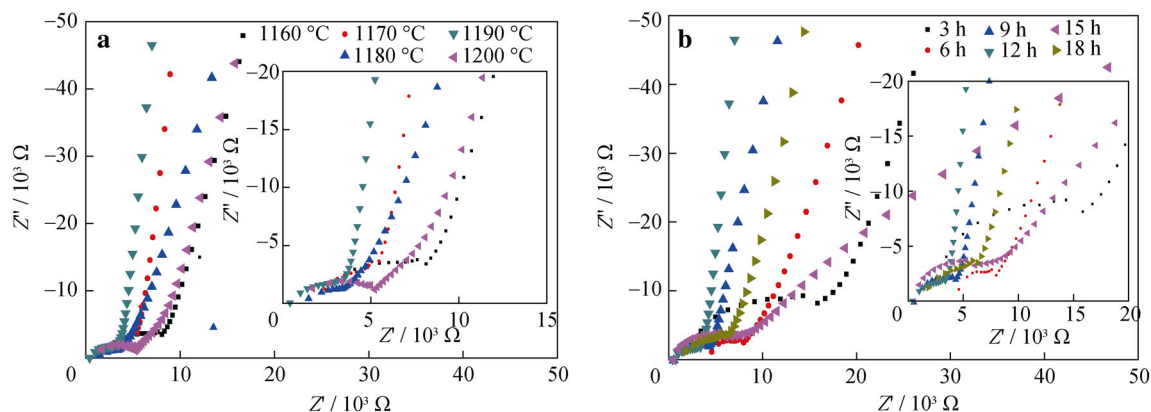
Fig. 4 Impedance spectra of Ba, Y and Al co-doped LLZO samples at **a** different temperatures and **b** different times measured at 25 °C (Z'- the real part of impedance, Z''- the imaginary part of impedance.)

Table 1 Conductivities of samples at different temperatures ($S \cdot cm^{-1}$)

1160 °C	1170 °C	1180 °C	1190 °C	1200 °C
1.23×10^{-5}	1.80×10^{-4}	2.75×10^{-4}	2.96×10^{-4}	1.92×10^{-4}

Table 2 Conductivities of samples at different time ($S \cdot cm^{-1}$)

| 3 h	6 h	9 h	12 h	15 h	18 h
6.29×10^{-5}	1.23×10^{-4}	2.33×10^{-4}	2.96×10^{-4}	1.99×10^{-4}	1.60×10^{-4}

Fig. 2a–d. It is beneficial for improving the ionic conductivity. With temperature changing from 1190 to 1200 °C, σ decreases from 2.96×10^{-4} to 1.92×10^{-4} $S \cdot cm^{-1}$; due to that as temperature further increases, small amounts of impurities such as $La_2Zr_2O_7$ are produced. The result is supported by XRD analysis result (Fig. 1a). And the results indicate that higher conductivities in the samples could be obtained by controlling temperature.

The impedance spectra of the Ba, Y and Al co-doped LLZO samples at different time measured at 25 °C in air are shown in Fig. 4b. From Fig. 4b, the plots of the samples show only a single semicircle at high frequency region and a remarkable diffusion tail at the low-frequency region. The total conductivity values of the samples are shown in Table 2.

From Table 2, σ increases significantly from 6.29×10^{-5} to 2.96×10^{-4} $S \cdot cm^{-1}$ with time increasing from 3 to 12 h; due to that as time increases, the grains contact better with each other. The result is supported by SEM analysis result in Fig. 3a–d. As time increases from 12 to 18 h, σ decreases from 2.96×10^{-4} to 1.60×10^{-4} $S \cdot cm^{-1}$; due to that as time further increases, the pores become more and bigger in the sample. The result is supported by SEM analysis result in Fig. 3d–f. And the results indicate that higher conductivities in the samples could be obtained by controlling time.

3.4 Relative density and contractibility rate

The relative density and contractibility rate of the Ba, Y and Al co-doped LLZO samples at different temperatures
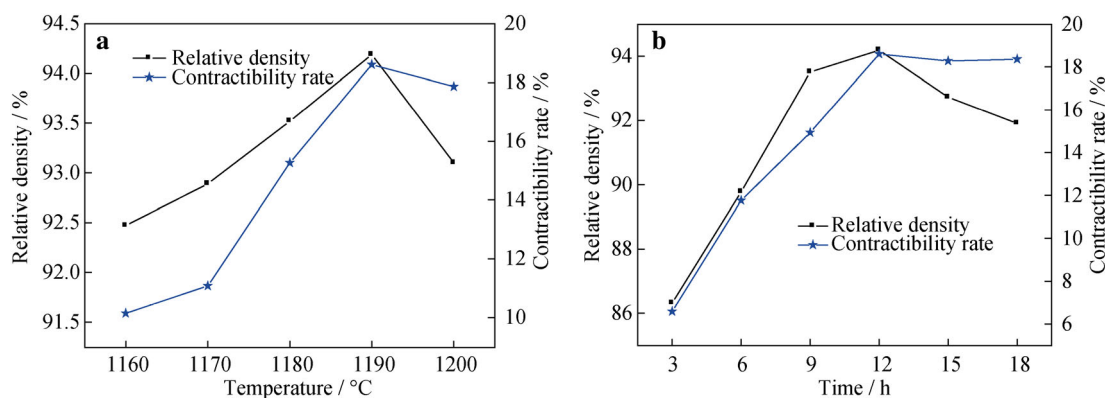
Fig. 5 Relative density and contractibility rate of Ba, Y and Al co-doped LLZO samples at **a** different temperatures and **b** different time

are shown in Fig. 5a. As can be seen, the relative density and contractibility rate increase from 92.47% and 10.15% to 94.19% and 18.61%, respectively, as temperature increases from 1160 to 1190 °C. As temperature increases from 1190 to 1200 °C, the relative density and contractibility rate decrease from 94.19% and 18.61% to 93.10% and 17.86%, respectively. The result is consistent with SEM and ionic conductivity analysis result.

The relative density and contractibility rate of the Ba, Y and Al co-doped LLZO samples at different time are shown in Fig. 5b. As can be seen, the relative density and contractibility rate increase significantly from 86.32% and 6.58% to 94.19% and 18.61%, respectively, with time changing from 3 to 12 h. As time changes from 12 to 18 h, the relative density and contractibility rate decrease from 94.19% and 18.61% to 91.91% and 18.37%, respectively. The result is consistent with SEM and ionic conductivity analysis result.

3.5 Composition

The composition of Ba, Y and Al co-doped LLZO sample (sintering at 1190 °C for 12 h) is shown in Table 3. As shown, Li:La:Ba:Zr:Y:O = 6.52:2.98:0.02:1.9:0.1:0.2:12 (atom fraction ratio), the composition of the sample is Li$_{6.52}$La$_{2.98}$Ba$_{0.02}$Zr$_{1.9}$Y$_{0.1}$Al$_{0.2}$O$_{12}$. Al was substituted in Li site in the formation process of the LLZO [18–20]. Alkali earth cations have been long considered to be confined exclusively to dodecahedral 8-coordinated sites (La sites) [3]. The ionic radius of Y^{3+}, Zr^{4+}, La^{3+} and Ba^{2+} are 0.088, 0.072, 0.103 and 0.135 nm, respectively. Because the ionic radius of Y^{3+} is the closest to that of Zr^{4+} among the ions, doping Y on Zr site is easier to occur. As shown in Table 3, the La:Ba molar ratio and Zr:Y molar ratio are 2.98:0.02 and 1.8:0.1, respectively, which well accords with the nominal stoichiometry and confirms the substitution of La and Zr sites with Ba^{2+} and Y^{3+}.

Table 3 Composition of sintered sample (1190 °C, 12 h)

Elements	Li	La	Ba	Zr	Y	Al	O
w/wt%	5.37	49.17	0.34	20.58	1.07	0.65	22.82
x/at%	6.52	2.98	0.02	1.90	0.10	0.20	12.00

4 Conclusion

The cubic garnet phase Ba, Y and Al co-doped LLZO is obtained, and the room-temperature total conductivity of the Ba, Y and Al co-doped LLZO solid electrolyte is improved significantly by eliminating the grain boundary resistances and improving the densifications with controlling temperature and time, respectively. Sintering at 1160–1190 °C for 12 h and for 6–15 h at 1190 °C, respectively, the Ba, Y and Al co-doped LLZO solid electrolytes are cubic garnet phase. Sintering at 1180–1190 °C for 12 h and for 12–18 h at 1190 °C, respectively, SEM images of the cross section of the Ba, Y and Al co-doped LLZO solid electrolytes exhibit the distinctively flattened morphology without any noticeable grain boundaries. The total conductivity, relative density and contractibility rate of Li$_{6.52}$La$_{2.98}$Ba$_{0.02}$Zr$_{1.9}$Y$_{0.1}$Al$_{0.2}$O$_{12}$ solid electrolyte are 2.96 × 10^{-4} S·cm^{-1}, 94.19% and 18.61%, respectively.

References

[1] Chen XL, Wang T, Lu WZ, Cao TX, Zhang CM. Synthesis of Ta and Ca doped Li$_7$La$_3$Zr$_2$O$_{12}$ solid-state electrolyte via simple solution method and its application in suppressing shuttle effect of Li–S battery. J Alloy Compd. 2018;744:386.

[2] Koshikawa H, Matsuda S, Kamiya K, Miyayama M, Nakanishi S. Dynamic changes in charge-transfer resistance at Li metal/$Li_7La_3Zr_2O_{12}$ interfaces during electrochemical Li dissolution/deposition cycles. J Power Sour. 2018;376:147.

[3] Chen XL, Cao TX, Xue MZ, Lu H, Zhang CM. Improved room temperature ionic conductivity of Ta and Ca doped $Li_7La_3Zr_2O_{12}$ via a modified solution method. Solid State Ion. 2018;314:92.

[4] Zhao PC, Cao GP, Jin ZQ, Ming H, Zhang ST. Self-consolidation mechanism and its application in the preparation of Al-doped cubic $Li_7La_3Zr_2O_{12}$. Mater Des. 2018;139:65.

[5] Han F, Yue J, Chen C, Zhao N, Fan X, Ma Z, Gao T, Wang F, Guo X, Wang C. Interphase engineering enabled all ceramic lithium battery. Joule. 2018;2:497.

[6] Zhang F, Shen F, Fan ZY, Ji X, Zhao B, Sun ZT, Xuan YY, Han XG. Ultrathin Al_2O_3-coated reduced graphene oxide membrane for stable lithium metal anode. Rare Met. 2018;37(6):510.

[7] Li T, Liu H, Shi P, Zhang Q. Recent progress in carbon/lithium metal composite anode for safe lithium metal batteries. Rare Met. 2018;37(6):449.

[8] Yang XF, Han XG, Chen ZP, Zhou LH, Jiao WZ. Improving the Li-ion conductivity and air stability of cubic $Li_7La_3Zr_2O_{12}$ by the co-doping of Nb, Y on the Zr site. J Eur Ceram Soc. 2018;38:1673.

[9] Yang XF, Han XG, Chen ZP, Zhou LH, Jiao WZ. Fabrication of $Li_7La_3Zr_2O_{12}$ fibers using bio-mass template Kapok. Mater Lett. 2018;217:271.

[10] Ramakumar S, Deviannapoorani C, Dhivya L. Lithium garnets: synthesis, structure, Li^+ conductivity, Li^+ dynamics and applications. Prog Mater Sci. 2017;88:325.

[11] Emil H, Wojciech Z, Li L. On fabrication procedures of Li-ion conducting garnets. J Solid State Chem. 2017;248:51.

[12] Murugan R, Thangadurai V, Weppner W. A thermally conductive separator for stable Li metal anodes. Angew Chem Int Ed. 2007;46:7778.

[13] Kotobuki M, Song SF, Takahashi R. Improvement of Li ion conductivity of $Li_5La_3Ta_2O_{12}$ solid electrolyte by substitution of Ge for Ta. J Power Sour. 2017;349:105.

[14] Kokal I, Somer M, Notten PHL. Sol-gel synthesis and lithium ion conductivity of $Li_7La_3Zr_2O_{12}$ with garnet-related type structure. Solid State Ion. 2011;185:42.

[15] Peng HJ, Feng LL, Li L. Synthesis of $Li_{5+x}La_3Hf_xNb_{2-x}O_{12}$ (x = 0.2–1) ceramics with cubic garnet-type structure. Mate-rials Lett. 2017;194:138.

[16] Shao CY, Yu ZY, Liu HX. Enhanced ionic conductivity of titanium doped $Li_7La_3Zr_2O_{12}$ solid electrolyte. Electrochim Acta. 2017;225:345.

[17] Andriyevsky B, Doll K, Jacob T. Ab initio molecular dynamics study of lithium diffusion in tetragonal $Li_7La_3Zr_2O_{12}$. Mater Chem Phys. 2017;185:210.

[18] Rosenkiewitz N, Schuhmacher J, Bockmeyer M. Nitrogen-free sol-gel synthesis of Al-substituted cubic garnet $Li_7La_3Zr_2O_{12}$ (LLZO). J Power Sour. 2015;278:104.

[19] Deviannapoorani C, Ramakumar S, Din MMU. Phase transition, lithium ion conductivity and structural stability of tin substituted lithium garnets. RSC Adv. 2016;6:94706.

[20] Zhang Y, Cai J, Chen F, Tu R, Shen Q, Zhang XL, Zhan LM. Preparation of cubic $Li_7La_3Zr_2O_{12}$ solid electrolyte using a nano-sized core-shell structured precursor. J Alloy Compd. 2015;644:793.

[21] Li YQ, Wang Z, Cao Y, Du M, Chen C, Cui ZH, Guo XX. W-doped $Li_7La_3Zr_2O_{12}$ ceramic electrolytes for solid state Li-ion batteries. Electrochim Acta. 2015;180:37.

[22] Allen JL, Wolfenstine J, Rangasamy E. Effect of substitution (Ta, Al, Ga) on the conductivity of $Li_7La_3Zr_2O_{12}$. J Power Sour. 2012;206:315.

[23] Dhivya L, Karthik K, Ramakumar S. Facile synthesis of high lithium ion conductive cubic phase lithium garnets for electro-chemical energy storage devices. RSC Adv. 2015;5:96042.

[24] Jiang Y, Zhu X, Qin S. Investigation of Mg^{2+}, Sc^{3+} and Zn^{2+} doping effects on densification and ionic conductivity of low-temperature sintered $Li_7La_3Zr_2O_{12}$ garnets. Solid State Ion. 2017;300:73.

[25] Peng HJ, Feng LL, Li L. Synthesis of $Li_{5+x}La_3Hf_xNb_{2x}O_{12}$ (x = 0.2–1) ceramics with cubic garnet-type structure. Mater Lett. 2017;194:138.

[26] Afyon S, Krumeich F, Rupp JLM. A shortcut to garnet-type fast Li-ion conductors for all-solid state batteries. J Mater Chem A. 2015;3:18636.

[27] Wang D, Zhong G, Dolotko O. The synergistic effects of Al and Te on the structure and Li^+-mobility of garnet-type solid electrolytes. J Mater Chem A. 2014;2:20271.

[28] Liu XZ, Liu YZ, Chen J. Preparation and application of the LiBaLaZrREAlO solid electrolyte. China Patent. CN 2016106059169, 2016.

[29] Rangasamy E, Wolfenstine J, Sakamoto J. Effect of substitution (Ta, Al, Ga) on the conductivity of $Li_7La_3Zr_2O_{12}$. Solid State Ion. 2012;206:315.

[30] Rangasamy E, Wolfenstine J, Allen J. The effect of 24c-site (A) cation substitution on the tetragonal-cubic phase transition in $Li_{7-x}La_{3-x}A_xZr_2O_{12}$ garnet-based ceramic electrolyte. J Power Sour. 2013;230:261.